



HAL
open science

Hyperbolic modeling of gradient damage and one-dimensional finite volume simulations

Nicolas Favrie, Adrien Renaud, Djimédo Kondo

► **To cite this version:**

Nicolas Favrie, Adrien Renaud, Djimédo Kondo. Hyperbolic modeling of gradient damage and one-dimensional finite volume simulations. 2023. hal-04237557

HAL Id: hal-04237557

<https://hal.science/hal-04237557>

Preprint submitted on 11 Oct 2023

HAL is a multi-disciplinary open access archive for the deposit and dissemination of scientific research documents, whether they are published or not. The documents may come from teaching and research institutions in France or abroad, or from public or private research centers.

L'archive ouverte pluridisciplinaire **HAL**, est destinée au dépôt et à la diffusion de documents scientifiques de niveau recherche, publiés ou non, émanant des établissements d'enseignement et de recherche français ou étrangers, des laboratoires publics ou privés.

Copyright

Hyperbolic modeling of gradient damage and one-dimensional finite volume simulations

Nicolas Favrie¹, Adrien Renaud¹, Djimedo Kondo²

¹ *Laboratoire IUSTI (Aix Marseille University, CNRS UMR 7343)
5 rue Enrico Fermi, 13453 Marseille, France
e-mail: {nicolas.favrie, adrien.renaud}@univ-amu.fr*

² *Institut Jean le Rond d'Alembert (Sorbonne Université, UPMC, CNRS UMR 7190)
4 Place Jussieu, 75005 Paris, France
e-mail: djimedo.kondo@sorbonne-universite.fr*

Abstract

This study provides a new formulation of gradient damage model which allows an efficient explicit numerical solution of dynamics problems. The proposed methodology is based on an "extended Lagrangian approach" developed by one of the authors for the nondissipative and dispersive shallow water equation. By using this strategy, the global minimization problem commonly derived for gradient damage models is recast as a purely local hyperbolic one with source terms that can be easily solved using finite volumes. The numerical solution of the governing system is then based on a fractional-step method consisting of a classical Godunov-type scheme and an implicit Ordinary Differential Equation solver for the local source terms. Numerical results are presented on the one-dimensional multi-fragmentation and spalling tests for illustration purpose.

Keywords: Brittle fracture; Dynamic fracture; Gradient damage; Hyperbolic models; Finite volumes.

1. Introduction

In continuum mechanics, damage theory introduced by KACHANOV aims at modeling the progressive degradation and failure of materials such as metals, concrete, rocks or glass. This framework is built upon the description of materials physical deterioration phenomena using a macroscopic damage variable (denoted as \mathcal{D} hereinafter) that is interpreted as microvoids and microcracks density parameter (see for instance [1]). KACHANOV, through the concept of *actual stress*, thus related the evolution of damage with the softening of materials. The notion of actual stress has later been abandoned in favor of thermodynamically consistent frameworks in which \mathcal{D} is an internal variable (see for instance [2, 3] in the context of Generalized Standard Materials framework [4]). This mainly led to interesting local constitutive damage models with isotropic or anisotropic damage variables [3, 5] or [6, 7] to cite a few.

When used to solve boundary value problems, the aforementioned models however lead to problems of existence and uniqueness of solutions and damage localization. As a conse-

quence, strong mesh dependencies are observed in numerical computations involving such local damage models. In that context, nonlocal models emerged in order to avoid the spurious localization problems. First, the equations related to the damage part of the problem have been reformulated by means of weighted volume averaged quantities such as the damage energy release rate in [8], or an equivalent strain measure in [9, 10] for instance. On the other hand, FRÉMOND and NEDJAR introduced the influence of damage at some material point to the constitutive response of its neighbors through the gradient of damage by considering the principle of virtual power [11, 12]. This type of gradient damage models falls within the framework of Generalized Standard Materials and has been later developed through several studies among which [13, 14]. Furthermore, variational formulations of gradient damage models [15] allowed to numerically solve brittle fracture problems by means of optimization techniques. In this perspective, an important step has been the seminal study of [16] followed by [17] which put emphasize on the convergence between regularized damage models and Griffith’s fracture theory in the asymptotic limit (see also [18]).

It is worth noticing that, in addition to the works mentioned above, the Thick Level Set [19] and the very recent Lip-field [20] approaches provide a regularization of local damage models based on geometrical constraints applied to the damage field.

Regularized damage mechanics models allow numerical simulations able to capture observed responses in quasi-static such as, for instance, a number of fragments. Nevertheless, difficulties arise in the context of dynamics. Indeed, in order to accurately follow the waves involved by dynamic loadings, numerical solutions based on explicit time discretization are preferable. This ability to track the waves however implies small time steps dictated by the CFL stability condition, enforcing that the fastest wave of the problem crosses at most the smallest mesh element, which is not the case with implicit approaches. In nonlinear solid mechanics, explicit Finite Element simulations are usually based on a staggered algorithm that requires at each time step: (1) the solution of the elastic problem on the mesh; (2) the implicit constitutive update at integration points. Gradient models as those used for regularized damage mechanics involve the solution of a nonlocal optimization problem in the second step of the staggered scheme [21–24]. Note that this is also true when using the TLS [25] and the Lip-Field [26]. Explicit dynamics obviously yields huge computational times for multi-dimensional calculations in nonlocal solids. In addition, the global optimization problem related to damage evolution makes it difficult to apply finite volume type schemes, which are known for their efficiency in following waves. This is in particular true in history dependent materials, for which finite element solutions suffer from spurious oscillations that lead to an overestimation of residual states [27].

In this paper, a new formulation allowing the efficient explicit numerical solution of dynamic problems in gradient damage solids is proposed. The derivation is based on the ”extended Lagrangian approach” originally developed by one of the author in [28] for the Serre–Green–Naghdi equation (shallow water equation with microinertia terms), in [29] for the defocusing Schrödinger equation (shallow water types equations with second gradient terms) or for bistable Ericksen bars [30]. Using this strategy, the original system with global minimization is recast as a purely local hyperbolic problem with source terms that can easily

be solved using finite volumes.

The approach proposed here being nonclassical, attention is paid to one-dimensional problems in the linearized geometrical limit only for simplicity. The extension to more general multi-dimensional finite deformations is straightforward after, however, many pages of calculation. In what follows, the thermodynamical formulation of the classical gradient damage model is recalled in section 2. Section 3 is then devoted to the derivation of the new model using Hamilton’s variational principle in the conservative context. Two terms bringing very small contributions to the Lagrangian functional will be introduced successively for clarity, one of them being already present in [12]. Dissipation is taken into account consistently with thermodynamics in section 4. The governing system thus obtained is hyperbolic with source terms, which is shown in section 5. The fractional-step method used to solve that system, consisting of a classical Godunov-type scheme using an approximate-state Riemann solver and an implicit Ordinary Differential Equation solver for the *local* source term, is also presented in section 5. Section 6 is dedicated to numerical results of one-dimensional multi-fragmentation and spalling tests. A conclusion is provided in section 7.

2. Constitutive model – Thermodynamics

The purpose of this section is the derivation of the damage evolution law used in section 3, within the associated Generalized Standard Materials framework. For the sake of generality, no explicit forms are yet assumed for the thermodynamics potentials. This point will be addressed in section 3.

Helmholtz free energy density

According to the classical approach for modeling gradient damage [12, 15] by means of internal variables [31], we consider, for one-dimensional problems in the linearized geometrical limit, the global Helmholtz free energy of a solid domain Ω of the form:

$$F = \int_{\Omega} \Psi(\boldsymbol{\varepsilon}(\mathbf{u}), \mathcal{D}, \nabla \mathcal{D}) d\Omega \quad (1)$$

where the free energy density Ψ depends on the infinitesimal strain $\boldsymbol{\varepsilon}$, the *damage field variable* \mathcal{D} and its gradient $\nabla \bullet = \frac{\partial \bullet}{\partial x}$, the dependence of Ψ on temperature being omitted here since we do not account for thermal aspects. The reader should note that, for the one-dimensional problems considered in this paper, the x subscript is also used for space derivatives with no ambiguity.

The authors insists on the fact that in the present context, \mathcal{D} and $\nabla \mathcal{D}$ are *not independent* variables since the damage variable \mathcal{D} is considered as a field.

As emphasized in [14], the geometrical relation between damage and its gradient leads, in the Generalized Standard Materials framework, to an over-constraining evolution law for internal variables. LORENTZ and ANDRIEUX [15] therefore proposed the definition of global

potentials. In particular, in the case of a nondissipative strain variable, the total dissipation results from the integration over the solid domain Ω of Clausius-Duhem inequality:

$$\mathbf{D} = - \int_{\Omega} \left(\frac{\partial \Psi}{\partial \mathcal{D}} \mathcal{D}_t + \frac{\partial \Psi}{\partial \nabla \mathcal{D}} \cdot \nabla \mathcal{D}_t \right) d\Omega \geq 0, \quad (2)$$

$(\bullet)_t$ denoting the time derivative in the remainder of the paper. After integration by parts and using the divergence theorem, the dissipation can be rewritten as:

$$\mathbf{D} = \int_{\Omega} \left(\operatorname{div} \frac{\partial \Psi}{\partial \nabla \mathcal{D}} - \frac{\partial \Psi}{\partial \mathcal{D}} \right) \mathcal{D}_t d\Omega - \int_{\partial\Omega} \left(\frac{\partial \Psi}{\partial \nabla \mathcal{D}} \cdot \mathbf{n} \right) \mathcal{D}_t ds \geq 0, \quad (3)$$

$\partial\Omega$ being the boundary of the solid domain. Note that, the boundary term vanishes according to natural boundary conditions so that the term involved in the volume integral thus defines the field of the thermodynamic force conjugated to the damage field \mathcal{D} :

$$\mathbf{Y}_{\mathcal{D}} = - \frac{\delta \Psi}{\delta \mathcal{D}} = \operatorname{div} \frac{\partial \Psi}{\partial \nabla \mathcal{D}} - \frac{\partial \Psi}{\partial \mathcal{D}} \quad (4)$$

where $\frac{\delta \Psi}{\delta \mathcal{D}}$ is the variational derivative of Ψ with respect to \mathcal{D} . Accordingly, the thermodynamic force $\mathbf{Y}_{\mathcal{D}}$ is nonlocal¹.

Dual dissipation pseudo-potential:

Restricting ourselves to the Generalized Standard Materials framework [4, 33, 34], we assume the existence of a dual dissipation pseudo-potential $\varphi^*(\mathbf{Y}_{\mathcal{D}})$, positive and convex with respect to the nonlocal thermodynamic force $\mathbf{Y}_{\mathcal{D}}$. This potential allows the derivation of the damage evolution law which reads:

$$\mathcal{D}_t = \frac{\partial \varphi^*}{\partial \mathbf{Y}_{\mathcal{D}}} \quad (5)$$

3. Derivation of the reversible model

In the following, we will first derive the nondissipative equations in a dynamic context as it can be made in fluid dynamics [35]. The dissipation related to irreversibility of damage will be addressed in the next section.

3.1. Hamilton's variational principle

In this section, the governing equations of the proposed model will be derived using Hamilton's principle in the context of conservative processes. A brief overview of this variational approach is first presented for readers who are not familiar with this formalism.

¹Such concept of nonlocal irreversible thermodynamic forces can be found in [32] where it has been called "space" Euler-Lagrange derivative with respect to \mathcal{D}

Consider a solid domain Ω with boundary $\partial\Omega$ of outward normal \mathbf{n} , submitted to volume and surface forces \mathbf{b} and \mathbf{t} within the time interval $\mathcal{T} = [t_1, t_2]$. Those actions will result in the displacement \mathbf{u} of the material points constituting the body with the velocity $\mathbf{v} = \mathbf{u}_t$. In the domain, the action integral is for isothermal evolutions the time integral of the Lagrangian \mathcal{L} defined below:

$$\mathcal{A} = \int_{\mathcal{T}} \mathcal{L} dt \quad (6)$$

with $\mathcal{L} = \mathcal{K} + \mathcal{W}_e - F$

in which thermal terms have been omitted. In addition to the Helmholtz free energy F , the potentials involved in the above functional are:

$$- \text{ the work of external forces } \mathcal{W}_e = \int_{\Omega} \mathbf{b} \cdot \mathbf{u} d\Omega + \int_{\partial\Omega} \mathbf{T}_d \cdot \mathbf{u} ds \quad (7)$$

$$- \text{ the kinetic energy } \mathcal{K} = \int_{\Omega} \frac{1}{2} \rho \mathbf{v} \cdot \mathbf{v} d\Omega \quad (8)$$

The Lagrangian is taken as a function of displacement and damage $(\mathbf{u}, \mathcal{D})$, of the damage gradient $\nabla\mathcal{D}$, and of velocity. The functional also depends on the infinitesimal strain tensor $\boldsymbol{\varepsilon} = \frac{1}{2} (\nabla\mathbf{u} + \nabla^T\mathbf{u})$, for which the following nonclassical form will be used:

$$\boldsymbol{\varepsilon} = \frac{1}{2} \operatorname{div} (\mathbf{u} \otimes \mathbf{I} + \mathbf{I} \boxtimes \mathbf{u}) \quad (9)$$

with $(\mathbf{a} \otimes \mathbf{I})_{ijk} = a_i \delta_{jk}$,
and $(\mathbf{I} \boxtimes \mathbf{a})_{ijk} = \delta_{ik} a_j \quad \forall \mathbf{a} \in \mathbb{R}^3$,

δ_{ij} being Kronecker delta symbol. This form allows the straightforward derivation of a geometrical conservation law [36] by simply taking the time partial derivative:

$$\boldsymbol{\varepsilon}_t - \operatorname{div} \left(\frac{\mathbf{v} \otimes \mathbf{I} + \mathbf{I} \boxtimes \mathbf{v}}{2} \right) = \mathbf{0}, \quad (10)$$

Hamilton's variational principle states that the evolution followed by the system satisfies the stationnarity of the action for any variation of the fields δu and $\delta \mathcal{D}$ that vanish on the boundary $\partial\mathcal{T}$. Namely:

$$\delta \mathcal{A} = \int_{\mathcal{T}} [\delta \mathcal{K} + \delta \mathcal{W}_e - \delta F] dt = 0 \quad (11)$$

After integrations by parts over space an time, and taking into account the vanishing variations on $\partial\mathcal{T}$ as well as equation (10), one gets:

$$\begin{aligned} \delta \mathcal{A} = & \int_{\mathcal{T}} \int_{\Omega} \left\{ \left[-\rho \mathbf{v}_t + \operatorname{div} \left(\frac{\partial \Psi}{\partial \boldsymbol{\varepsilon}} \right) + \mathbf{b} \right] \cdot \delta \mathbf{u} + \left[\operatorname{div} \left(\frac{\partial \Psi}{\partial \nabla \mathcal{D}} \right) - \frac{\partial \Psi}{\partial \mathcal{D}} \right] \delta \mathcal{D} \right\} d\Omega dt \\ & + \int_{\mathcal{T}} \int_{\partial\Omega} \left\{ \left[-\frac{\partial \Psi}{\partial \boldsymbol{\varepsilon}} \cdot \mathbf{n} + \mathbf{T}_d \right] \cdot \delta \mathbf{u} + \left[\frac{\partial \Psi}{\partial \nabla \mathcal{D}} \cdot \mathbf{n} \right] \delta \mathcal{D} \right\} ds dt = 0 \quad \forall \delta \mathbf{u}, \delta \mathcal{D} \end{aligned} \quad (12)$$

Notice that the thermodynamic force associated with damage $Y_{\mathcal{D}} = \operatorname{div} \left(\frac{\partial \Psi}{\partial \nabla \mathcal{D}} \right) - \frac{\partial \Psi}{\partial \mathcal{D}}$ naturally arises in the volume integral.

Considering first variations $\delta \mathbf{u}$ and $\delta \mathcal{D}$ that are both zero on $\partial \Omega$, we are left with the following condition in the volume Ω :

$$\left[-\rho \mathbf{v}_t + \operatorname{div} \left(\frac{\partial \Psi}{\partial \boldsymbol{\varepsilon}} \right) + \mathbf{b} \right] \cdot \delta \mathbf{u} + Y_{\mathcal{D}} \delta \mathcal{D} = 0 \quad \forall \delta \mathbf{u}, \delta \mathcal{D} \quad (13)$$

Taking $\delta \mathcal{D} = 0$ implies that the first term must be zero regardless of the value of $\delta \mathbf{u}$, which yields the balance equation of linear momentum:

$$\rho \mathbf{v}_t - \operatorname{div} \boldsymbol{\sigma} = \mathbf{b}, \quad \text{with } \boldsymbol{\sigma} = \frac{\partial \Psi}{\partial \boldsymbol{\varepsilon}} \quad (14)$$

The above equation leads in (13) to the conclusion $Y_{\mathcal{D}} \delta \mathcal{D} = 0 \quad \forall \delta \mathcal{D}$. Since $Y_{\mathcal{D}}$ depends on the displacement and the damage variable, as we shall see later, one can imagine elastic evolutions ($\mathbf{u} \neq \mathbf{0}$, $\mathcal{D}_t = 0$) for which $Y_{\mathcal{D}} \neq 0$. The equality $Y_{\mathcal{D}} = 0$ can then only be satisfied if damage varies ($\mathcal{D}_t \neq 0$) to accommodate the displacement contribution. From the previous reasoning, the last equation is derived:

$$\left[\operatorname{div} \left(\frac{\partial \Psi}{\partial \nabla \mathcal{D}} \right) - \frac{\partial \Psi}{\partial \mathcal{D}} \right] \mathcal{D}_t = 0 \quad (15)$$

which involves that the total dissipation (3) is zero according to the nondissipative framework. The derived volume equations are recalled below for convenience:

$$\left\{ \begin{array}{l} \boldsymbol{\varepsilon}_t - \operatorname{div} \left(\frac{\mathbf{v} \otimes \mathbf{I} + \mathbf{I} \otimes \mathbf{v}}{2} \right) = \mathbf{0} \\ \rho \mathbf{v}_t - \operatorname{div} \boldsymbol{\sigma} = \mathbf{b} \\ \left[\operatorname{div} \left(\frac{\partial \Psi}{\partial \nabla \mathcal{D}} \right) - \frac{\partial \Psi}{\partial \mathcal{D}} \right] \mathcal{D}_t = 0 \end{array} \right. \quad \forall \mathbf{x} \in \Omega \quad (16)$$

For variations $\delta \mathbf{u} = \mathbf{0}$ and $\delta \mathcal{D} = 0$ in Ω , and assuming that $\frac{\partial \Psi}{\partial \nabla \mathcal{D}}$ does not depend on the displacement, the following boundary conditions are derived:

$$\left\{ \begin{array}{l} \boldsymbol{\sigma} \cdot \mathbf{n} = \mathbf{T}_d \\ \frac{\partial \Psi}{\partial \nabla \mathcal{D}} \cdot \mathbf{n} = 0 \end{array} \right. \quad \forall \mathbf{x} \in \partial \Omega \quad (17)$$

The first equation corresponds to classical Neumann boundary conditions, and the second one leads to a vanishing boundary integral in the dissipation (3).

Denoting the internal energy density by $e(\boldsymbol{\varepsilon}, \mathcal{D}, \nabla \mathcal{D})$, the rate of change of the total energy density E can be written as:

$$E_t = \frac{d}{dt} \left(\frac{1}{2} \rho \|\mathbf{v}\|^2 \right) + e_t \quad (18)$$

Since the partial derivatives of e with respect to $\boldsymbol{\varepsilon}$, \mathcal{D} and $\nabla\mathcal{D}$ are the same as those of Ψ for isothermal processes, the total energy balance law reads after taking into account the linear momentum balance:

$$E_t - \operatorname{div} \left(\frac{\partial\Psi}{\partial\boldsymbol{\varepsilon}} \cdot \mathbf{v} + \frac{\partial\Psi}{\partial\nabla\mathcal{D}} \mathcal{D}_t \right) = - \left[\operatorname{div} \left(\frac{\partial\Psi}{\partial\nabla\mathcal{D}} \right) - \frac{\partial\Psi}{\partial\mathcal{D}} \right] \mathcal{D}_t + \mathbf{b} \cdot \mathbf{v} \quad (19)$$

where the term $\frac{\partial\Psi}{\partial\nabla\mathcal{D}} \mathcal{D}_t$ is called *interstitial working* [37].

Combination of equations (19) and (15) shows that energy is conserved in absence of external volume forces (as will be considered hereinafter). This is consistent with our first goal of deriving the nondissipative model.

In what follows, the same approach is used for different choices of the Lagrangian functional.

3.2. Master Lagrangian

We start the derivation with the classical form of the kinetic energy density, and a free energy density widely used for the quasi-static modeling of gradient damage (see for instance [14]):

$$\Psi(\boldsymbol{\varepsilon}, \mathcal{D}, \nabla\mathcal{D}) = \frac{1}{2} \boldsymbol{\varepsilon} : \mathbb{C}(\mathcal{D}) : \boldsymbol{\varepsilon} + w(\mathcal{D}) + \frac{1}{2} \mathbf{w}_{l_c} l_c^2 \|\nabla\mathcal{D}\|^2 \quad (20)$$

In (20), the first term is the elastic energy in which $\mathbb{C}(\mathcal{D})$ is the damage-dependent fourth-order stiffness tensor, $w(\mathcal{D})$ is the local damage energy and the last term is the nonlocal damage energy involving a characteristic length l_c and a material constant $\mathbf{w}_{l_c} > 0$.

It is worth noticing that both local and nonlocal damage energies are in this definition *stored energies*. Once again, we focus for now on the nondissipative modeling and postpone to section 4 the possibility of *tuning* the stored and dissipated parts.

Specialization of system (16) and of the energy balance equation (19) to the above free energy density yields respectively:

$$\left\{ \begin{array}{l} \boldsymbol{\varepsilon}_t - \operatorname{div} \left(\frac{\mathbf{v} \otimes \mathbf{I} + \mathbf{I} \boxtimes \mathbf{v}}{2} \right) = \mathbf{0} \\ \rho \mathbf{v}_t - \operatorname{div} \boldsymbol{\sigma} = \mathbf{0} \quad \text{with} \quad \boldsymbol{\sigma} = \mathbb{C}(\mathcal{D}) : \boldsymbol{\varepsilon} \\ \left(\frac{1}{2} \boldsymbol{\varepsilon} : \mathbb{C}'(\mathcal{D}) : \boldsymbol{\varepsilon} + w'(\mathcal{D}) - \mathbf{w}_{l_c} l_c^2 \Delta\mathcal{D} \right) \mathcal{D}_t = -Y_{\mathcal{D}} \mathcal{D}_t = 0, \end{array} \right. \quad \forall \mathbf{x} \in \Omega \quad (21)$$

and:

$$E_t - \operatorname{div} (\boldsymbol{\sigma} \cdot \mathbf{v} + \mathbf{w}_{l_c} l_c^2 (\nabla\mathcal{D}) \mathcal{D}_t) = \left(\frac{1}{2} \boldsymbol{\varepsilon} : \mathbb{C}'(\mathcal{D}) : \boldsymbol{\varepsilon} + w'(\mathcal{D}) - \mathbf{w}_{l_c} l_c^2 \Delta\mathcal{D} \right) \mathcal{D}_t = -Y_{\mathcal{D}} \mathcal{D}_t = 0 \quad (22)$$

In addition, the natural boundary conditions are:

$$\left\{ \begin{array}{l} \boldsymbol{\sigma} \cdot \mathbf{n} = \mathbf{T}_d \\ \mathbf{w}_{l_c} l_c^2 \nabla\mathcal{D} \cdot \mathbf{n} = 0 \end{array} \right. \quad \forall \mathbf{x} \in \partial\Omega \quad (23)$$

The derived set of equations (21) is very difficult to solve in the explicit dynamics context. Indeed, solving a Laplace equation in zones where damage increases such as dictated by (21)₃ is prohibitive numerically speaking, especially for multi-dimensional problems.

3.3. Extended Lagrangian

To get rid of the resolution of Laplace equation, we introduce a microinertia term in the Lagrangian as proposed by [12]. In this case, the kinetic energy reads:

$$K = \int_{\Omega} \left(\frac{1}{2} \rho \|\mathbf{v}\|^2 + \frac{1}{2} \beta \mathcal{D}_t^2 \right) d\Omega \quad (24)$$

The microinertia parameter β is assumed small and is introduced here as an extension of the inertia of microvoids observed in ductile fracture [38] to brittle fracture. To be complete, the introduction of microinertia should be done by taking β as a function of damage. Nevertheless the microinertia parameter is constant in this work for simplicity, which is not a limitation of the model but only a choice.

The governing system is in that case:

$$\left\{ \begin{array}{l} \boldsymbol{\varepsilon}_t - \operatorname{div} \left(\frac{\mathbf{v} \otimes \mathbf{I} + \mathbf{I} \boxtimes \mathbf{v}}{2} \right) = \mathbf{0} \\ \rho \mathbf{v}_t - \operatorname{div} \boldsymbol{\sigma} = \mathbf{0} \quad \text{with} \quad \boldsymbol{\sigma} = \mathbb{C}(\mathcal{D}) : \boldsymbol{\varepsilon} \\ \left(\frac{1}{2} \boldsymbol{\varepsilon} : \mathbb{C}'(\mathcal{D}) : \boldsymbol{\varepsilon} + w'(\mathcal{D}) - w_{l_c} l_c^2 \Delta \mathcal{D} + \beta \mathcal{D}_{tt} \right) \mathcal{D}_t = 0 \end{array} \right. \quad \forall \mathbf{x} \in \Omega \quad (25)$$

The energy conservation law can also be rewritten as a consequence:

$$E_t - \operatorname{div} \left(\boldsymbol{\sigma} \cdot \mathbf{v} + w_{l_c} l_c^2 (\nabla \mathcal{D}) \mathcal{D}_t \right) = \left(\frac{1}{2} \boldsymbol{\varepsilon} : \mathbb{C}'(\mathcal{D}) : \boldsymbol{\varepsilon} + w'(\mathcal{D}) - w_{l_c} l_c^2 \Delta \mathcal{D} + \beta \mathcal{D}_{tt} \mathcal{D} \right) \mathcal{D}_t = 0, \quad (26)$$

along with the boundary conditions:

$$\left\{ \begin{array}{l} \boldsymbol{\sigma} \cdot \mathbf{n} = \mathbf{T}_d \\ w_{l_c} l_c^2 \nabla \mathcal{D} \cdot \mathbf{n} = 0 \end{array} \right. \quad \forall \mathbf{x} \in \partial\Omega \quad (27)$$

When $\mathcal{D}_t \neq 0$, the terms in the parenthesis in equation (25)₃ becomes an hyperbolic equation with source terms. However, this equation being only valid when damage evolves, it is not convenient for numerical resolution. In addition, anticipating on damage evolution, the yield surface depends on the thermodynamic force $\mathbf{Y}_{\mathcal{D}}$ which, as seen in the third equation of system (25), is a function of the Laplacian of \mathcal{D} . This is something we want to avoid.

In order to circumvent this issue we propose a two-field modeling analogous to the *micro-morphic* approach [39–41], based on the introduction of an additional *nondissipative* variable

$\tilde{\mathcal{D}}$. The Lagrangian then becomes a function of $\boldsymbol{\varepsilon}$, \mathcal{D} , $\tilde{\mathcal{D}}$, $\tilde{\mathcal{D}}_t$ and $\nabla\tilde{\mathcal{D}}$, and the kinetic and free energies now read:

$$K = \int_{\Omega} \left(\frac{1}{2} \rho \|\mathbf{v}\|^2 + \frac{1}{2} \beta \tilde{\mathcal{D}}_t^2 \right) d\Omega \quad (28)$$

$$F = \int_{\Omega} \left[\frac{1}{2} \boldsymbol{\varepsilon} : \mathbb{C}(\mathcal{D}) : \boldsymbol{\varepsilon} + w(\mathcal{D}) + \frac{1}{2} \mathbf{w}_{l_c} l_c^2 \|\nabla\tilde{\mathcal{D}}\|^2 + \frac{\kappa}{2} (\tilde{\mathcal{D}} - \mathcal{D})^2 \right] d\Omega \quad (29)$$

Notice that in the classical micromorphic approach, the term $(\tilde{\mathcal{D}} - \mathcal{D})$ is a relative generalized damage variable which, in this work, is constrained to vanish by ascribing a large value to the parameter κ , thus providing the latter the role of a penalty parameter. This constraint allows recovering the gradient damage formulation commonly used. The same approach has been used in [28–30] for various classes of dispersive equations such as Serre–Green–Naghdi, Schrödinger equation and bistable Ericksen bar.

The application of Hamilton’s principle on that *extended Lagrangian* yields an additional equation corresponding to the variation of $\tilde{\mathcal{D}}$. The governing system is then:

$$\begin{cases} \boldsymbol{\varepsilon}_t - \operatorname{div} \left(\frac{\mathbf{v} \otimes \mathbf{I} + \mathbf{I} \otimes \mathbf{v}}{2} \right) = \mathbf{0} \\ \rho \mathbf{v}_t - \operatorname{div} \boldsymbol{\sigma} = \mathbf{0} \quad \text{with } \boldsymbol{\sigma} = \mathbb{C}(\mathcal{D}) : \boldsymbol{\varepsilon} \\ \left(\frac{1}{2} \boldsymbol{\varepsilon} : \mathbb{C}'(\mathcal{D}) : \boldsymbol{\varepsilon} + w'(\mathcal{D}) - \kappa (\tilde{\mathcal{D}} - \mathcal{D}) \right) \mathcal{D}_t = 0 \\ \beta \tilde{\mathcal{D}}_{tt} - \mathbf{w}_{l_c} l_c^2 \Delta \tilde{\mathcal{D}} = -\kappa (\tilde{\mathcal{D}} - \mathcal{D}) \end{cases} \quad \forall \mathbf{x} \in \Omega \quad (30)$$

The energy conservation law reads:

$$E_t - \operatorname{div} \left(\boldsymbol{\sigma} \cdot \mathbf{v} + \mathbf{w}_{l_c} l_c^2 (\nabla\tilde{\mathcal{D}}) \tilde{\mathcal{D}}_t \right) = \left(\frac{1}{2} \boldsymbol{\varepsilon} : \mathbb{C}'(\mathcal{D}) : \boldsymbol{\varepsilon} + w'(\mathcal{D}) - \kappa (\tilde{\mathcal{D}} - \mathcal{D}) \right) \mathcal{D}_t = 0, \quad (31)$$

and the boundary conditions are now:

$$\begin{cases} \boldsymbol{\sigma} \cdot \mathbf{n} = \mathbf{T}_d \\ \mathbf{w}_{l_c} l_c^2 \nabla\tilde{\mathcal{D}} \cdot \mathbf{n} = 0 \end{cases} \quad \forall \mathbf{x} \in \partial\Omega \quad (32)$$

Notice that since equation (30)₄ does not depend on \mathbf{u} , there is no need to consider the special cases $\tilde{\mathcal{D}}_t = 0$ or $\tilde{\mathcal{D}}_t \neq 0$ as has been done for equation (30)₃.

Combination of equations (30)₃ and (30)₄ leads to the following expression of the thermodynamic force associated with damage:

$$\Upsilon_{\mathcal{D}} = -\frac{1}{2} \boldsymbol{\varepsilon} : \mathbb{C}'(\mathcal{D}) : \boldsymbol{\varepsilon} - w'(\mathcal{D}) - \beta \tilde{\mathcal{D}}_{tt} + \mathbf{w}_{l_c} l_c^2 \Delta \tilde{\mathcal{D}} \quad (33)$$

Hence, for sufficiently large values of the penalty parameter (*i.e.* $\tilde{\mathcal{D}} \rightarrow \mathcal{D}$) and in the microinertia-vanishing limit $\beta \rightarrow 0$, the extended Lagrangian allows recovering the classical definition of $\Upsilon_{\mathcal{D}}$ (4).

4. Introduction of the dissipation and formulation of the gradient damage model

4.1. Damage evolution equation

We will now complete the reversible model presented in section 3 by adding the evolution law of damage. Let's consider a convex dual potential $\varphi^*(\mathbf{Y}_{\mathcal{D}})$. The damage evolution law is defined as:

$$\mathcal{D}_t = \frac{\partial \varphi^*}{\partial \mathbf{Y}_{\mathcal{D}}} \quad (34)$$

For instance, without loss of generality one possible choice is:

$$\varphi^* = \frac{\langle f_{\mathcal{D}}(\mathbf{Y}_{\mathcal{D}}) \rangle^2}{2\eta} \quad (35)$$

where $\langle f \rangle$ is the positive part of f and η is the viscosity. With such a choice, the evolution equation on the damage variable is:

$$\mathcal{D}_t = \frac{\langle f_{\mathcal{D}}(\mathbf{Y}_{\mathcal{D}}) \rangle}{\eta} \frac{\partial f_{\mathcal{D}}(\mathbf{Y}_{\mathcal{D}})}{\partial \mathbf{Y}_{\mathcal{D}}} \quad (36)$$

Notice that as $\eta \rightarrow 0$, the model retrieves the rate-independent limit (*i.e.* the consistency condition $f_{\mathcal{D}} \mathcal{D}_t = 0$ is satisfied).

Depending on the form given to the yield function, both nondissipative $\mathbf{Y}_{\mathcal{D}} \mathcal{D}_t = 0$ and dissipative $\mathbf{Y}_{\mathcal{D}} \mathcal{D}_t > 0$ cases can be considered. This is shown in section 4.2.

Replacing the zero dissipation equation (30)₃ by the damage evolution law, the governing equations in presence of dissipation are:

$$\left\{ \begin{array}{l} \boldsymbol{\varepsilon}_t - \operatorname{div} \left(\frac{\mathbf{v} \otimes \mathbf{I} + \mathbf{I} \boxtimes \mathbf{v}}{2} \right) = \mathbf{0} \\ \rho \mathbf{v}_t - \operatorname{div} \boldsymbol{\sigma} = \mathbf{0} \text{ with } \boldsymbol{\sigma} = \mathbb{C}(\mathcal{D}) : \boldsymbol{\varepsilon} \\ \mathcal{D}_t = \frac{\partial \varphi^*}{\partial \mathbf{Y}_{\mathcal{D}}} \\ \beta \tilde{\mathcal{D}}_{tt} - \mathbf{w}_{l_c} l_c^2 \Delta \tilde{\mathcal{D}} = -\kappa(\tilde{\mathcal{D}} - \mathcal{D}), \end{array} \right. \quad \forall \mathbf{x} \in \Omega \quad (37)$$

and the energy conservation law reads:

$$E_t - \operatorname{div} \left(\boldsymbol{\sigma} \cdot \mathbf{v} + \mathbf{w}_{l_c} l_c^2 (\nabla \tilde{\mathcal{D}}) \tilde{\mathcal{D}}_t \right) = \left(\frac{1}{2} \boldsymbol{\varepsilon} : \mathbb{C}'(\mathcal{D}) : \boldsymbol{\varepsilon} + w'(\mathcal{D}) - \kappa(\tilde{\mathcal{D}} - \mathcal{D}) \right) \mathcal{D}_t = -\mathbf{Y}_{\mathcal{D}} \frac{\partial \varphi^*}{\partial \mathbf{Y}_{\mathcal{D}}} \leq 0 \quad (38)$$

4.2. Examples

In this subsection, two damage model formulations used in one of the numerical simulations discussed in section 6 are presented. From now on, attention is only paid to one-dimensional problems for simplicity and clarity. The partial derivatives with respect to

the space coordinate x are then denoted as $\frac{\partial \bullet}{\partial x} = (\bullet)_x$ and stress and strain are respectively written σ and ε .

For both examples, the free energy density reads:

$$\Psi = \frac{A(\mathcal{D})}{2}\varepsilon^2 + w(\mathcal{D}) + \frac{1}{2}w_{lc}l_c^2\tilde{\mathcal{D}}_x^2 + \frac{\kappa}{2}(\tilde{\mathcal{D}} - \mathcal{D})^2 \quad (39)$$

where $A(\mathcal{D})$ is the elastic stiffness.

To illustrate the flexibility of the model, particular forms are considered for the local damage energy and the damage yield function [12, 42].

4.2.1. Example 1: Dissipative model

In this first example, we consider:

$$w(\mathcal{D}) = -M_l(\ln(1 - \mathcal{D}) + \mathcal{D}), \quad M_l \geq 0 \quad (40)$$

$$\varphi^*(\mathbf{Y}_{\mathcal{D}}) = \frac{\langle f_{\mathcal{D}}(\mathbf{Y}_{\mathcal{D}}) \rangle^2}{2\eta} \quad (41)$$

$$f_{\mathcal{D}} \equiv \mathbf{Y}_{\mathcal{D}} - k_l = -A'(\mathcal{D})\frac{\varepsilon^2}{2} + \kappa(\tilde{\mathcal{D}} - \mathcal{D}) + M_l\frac{\mathcal{D}}{1 - \mathcal{D}} - k_l, \quad k_l \geq 0 \quad (42)$$

In the above model, k_l is the initial damage threshold and the logarithmic part of the local damage energy ensures $\mathcal{D} < 1$ ($\mathcal{D} = 1$ leads to an infinite energy).

According to the dissipation expression (3), one has in that case:

$$\mathcal{D} = \int_{\Omega} \eta \frac{f_{\mathcal{D}} + k_l}{\langle f_{\mathcal{D}} \rangle} \mathcal{D}_t^2 d\Omega \quad (43)$$

which, even for small values of η , is nonzero when damage has increased due to the term k_l .

4.2.2. Example 2: nondissipative model

Alternatively, the following model can be used:

$$w(\mathcal{D}) = k_l\mathcal{D} - M_l(\ln(1 - \mathcal{D}) + \mathcal{D}), \quad M_l, k_l \geq 0 \quad (44)$$

$$\varphi^*(\mathbf{Y}_{\mathcal{D}}) = \frac{\langle f_{\mathcal{D}}(\mathbf{Y}_{\mathcal{D}}) \rangle^2}{2\eta} \quad (45)$$

$$f_{\mathcal{D}} \equiv \mathbf{Y}_{\mathcal{D}} = -A'(\mathcal{D})\frac{\varepsilon^2}{2} + \kappa(\tilde{\mathcal{D}} - \mathcal{D}) + M_l\frac{\mathcal{D}}{1 - \mathcal{D}} - k_l \quad (46)$$

In that case, the evolution of damage will be identical to the previous model considered for the yield function has the same expression. Nevertheless, the dissipation reads:

$$\mathcal{D} = \int_{\Omega} \eta \frac{f_{\mathcal{D}}}{\langle f_{\mathcal{D}} \rangle} \mathcal{D}_t^2 d\Omega \quad (47)$$

which, for sufficiently small values of the relaxation parameter η , is zero. Indeed, the consistency condition $f_{\mathcal{D}}\mathcal{D}_t = 0$ is recovered in that case.

The reader shall note that even if the local damage energy $w(\mathcal{D})$ has two different expressions in the above examples, it is not the case for the yield function $f_{\mathcal{D}}$. As a result, the damage variable evolution is the same in both cases, leading to $\sigma - \varepsilon$ curves that are identical .

Similar manipulations can be made to include a contribution of the damage gradient in the dissipation by working on the term $\kappa(\tilde{\mathcal{D}} - \mathcal{D})$ in the free energy. This is, however, not considered here.

5. Numerical solution

In this section, and as already indicated, we restrict ourselves to the 1D case, the hyperbolicity of the governing system is shown and the numerical solution procedure based on finite volumes is briefly presented. This will allow to show some predictive capability of the model.

Gathering all the ingredients developed above and making use of the change of variable $q = \tilde{\mathcal{D}}_t$ and $p = \tilde{\mathcal{D}}_x$, the governing system, specialized to one space dimension, is recast as:

$$\begin{cases} \varepsilon_t - v_x = 0 \\ \rho v_t - \sigma_x = 0 \\ \mathcal{D}_t = \frac{\partial \varphi^*}{\partial \mathcal{Y}_{\mathcal{D}}} \\ \tilde{\mathcal{D}}_t = q \\ \beta q_t - \mathbf{w}_{l_c} l_c^2 p_x = -\kappa(\tilde{\mathcal{D}} - \mathcal{D}) \\ p_t - q_x = 0 \end{cases} \quad (48)$$

The last equation in this system expresses Schwarz mixed partial derivatives theorem for the variables p and q .

Using the array vector notation, system (48) is written in the following form:

$$\begin{aligned} \mathbf{U}_t + \mathbf{F}(\mathbf{U})_x &= \mathbf{S}(\mathbf{U}), \\ \mathbf{U} &= [\varepsilon, \rho v, \mathcal{D}, \tilde{\mathcal{D}}, \beta q, p]^T, \\ \mathbf{F} &= [-v, -\sigma, 0, 0, -\mathbf{w}_{l_c} l_c^2 p, -q]^T, \\ \mathbf{S} &= \left[0, 0, \frac{1}{\tau} \langle f_{\mathcal{D}} \rangle, q, -\kappa(\tilde{\mathcal{D}} - \mathcal{D}), 0 \right]^T \end{aligned} \quad (49)$$

To solve this system, a fractional-step method will be applied [43]. This consists in solving the homogeneous system and a system of Ordinary Differential Equations (ODE) associated with the source term in a staggered fashion. Such a procedure can be seen as a predictor–corrector approach in which damage flow can only occur in the ODE.

5.1. Hyperbolicity

The Riemann problem associated with system (49) consists of the quasi-linear form of its homogeneous part and initial conditions on the vector of conserved quantities \mathbf{U} :

$$\mathbf{U}_t + \frac{\partial \mathbf{F}(\mathbf{U})}{\partial \mathbf{U}} \mathbf{U}_x = 0, \quad \text{with} \quad \begin{cases} \mathbf{U}(x, t = 0) = \mathbf{U}_L & \text{if } x < 0 \\ \mathbf{U}(x, t = 0) = \mathbf{U}_R & \text{if } x > 0 \end{cases} \quad (50)$$

In (50), the Jacobian matrix $\mathbf{J} = \frac{\partial \mathbf{F}(\mathbf{U})}{\partial \mathbf{U}}$ arises from the chain rule and the subscripts R and L denote quantities defined on the Right and Left side of the initial discontinuity located at $x = 0$ respectively.

The hyperbolicity condition of this system relies on the eigenvalues and eigenvectors of \mathbf{J} that must respectively be real and form an complete basis. For the block diagonal Jacobian matrix under consideration, it is easy to show that there are four nonzero eigenvalues:

$$c_{R,L}^E = \pm \sqrt{\frac{A(\mathcal{D}_{R,L})}{\rho}} \quad ; \quad c_{R,L}^D = \pm \sqrt{\frac{\mathbf{w}_c l_c^2}{\beta}} \quad (51)$$

The eigenvalues $c_{R,L}^E$ correspond to the classical elastic wave speeds and $c_{R,L}^D$ are the wave speeds associated with the transport equation of the additional damage variable $\tilde{\mathcal{D}}$.

There are three remarks about the characteristic structure of the solutions of system (49):

1. Since damage does not increase in the homogeneous system (*i.e.* $\mathcal{D}_t = 0$), both characteristic speeds are constant. For the "damage speeds" c^D , however, this due to the choice of a constant microinertia parameter β and will be no longer true for $\beta \equiv \beta(\tilde{\mathcal{D}})$.
2. Given that the eigenvalues are real and one can define a complete set of independent eigenvectors, system (49) is hyperbolic.
3. The quasi-linear form (50) shows that the problem can be decoupled into a purely elastic part involving waves of speeds $c_{R,L}^E$ on the one hand, and a pure transport of the additional damage variable at speeds $c_{R,L}^D$.

Since the Riemann problem can be decoupled, one then has to solve:

$$\mathbf{W}_t + \frac{\partial \bar{\mathbf{F}}(\mathbf{W})}{\partial \mathbf{W}} \mathbf{W}_x = 0, \quad \text{with} \quad \begin{cases} \mathbf{W}(x, t = 0) = \mathbf{W}_L & \text{if } x < 0 \\ \mathbf{W}(x, t = 0) = \mathbf{W}_R & \text{if } x > 0 \end{cases} \quad (52)$$

for $\mathbf{W} = [\varepsilon, \rho v]^T$; $\bar{\mathbf{F}} = [-v, -\sigma]^T$ and $\mathbf{W} = [\beta q, p]^T$; $\bar{\mathbf{F}} = [-\mathbf{w}_c l_c^2 p, -q]^T$. Figure 1 shows the characteristic structure of the solution of one of those Riemann problem. Owing to the initial discontinuity between \mathbf{W}_L and \mathbf{W}_R in the Riemann problem, two waves propagate leftward and rightward while carrying a jump discontinuity that result in a constant *stationary state* \mathbf{W}^* after the passage of waves.

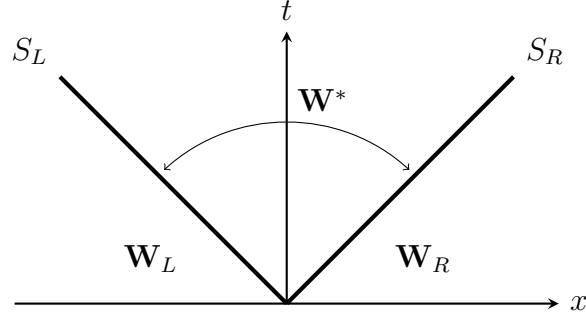


Figure 1: Characteristic structure of the solution of each decoupled Riemann problem: waves with speeds S_\bullet carrying jump discontinuities $\mathbf{W}_\bullet^* - \mathbf{W}_\bullet$.

5.2. Solution of the homogeneous system

Considering a partition of the one-dimensional domain Ω by means of N_c finite volume cells, a piece-wise constant approximation of \mathbf{U} can be constructed in Ω . With, in addition, an explicit Euler time discretization, the homogeneous part of system (49) can be discretized in space and time for cell i between times t^n and t^{n+1} as:

$$\mathbf{U}_i^{n+1} = \mathbf{U}_i^n - \frac{\Delta t^n}{\Delta x_i} (\mathbf{F}_{i+1/2}^* - \mathbf{F}_{i-1/2}^*) \quad \forall i \quad (53)$$

In equation (53), $\mathbf{F}_{i\pm 1/2}^*$ are fluxes computed at the interface between cells i and $i \pm 1$ that result from the discontinuity of \mathbf{U} in the piece-wise constant approximation. These terms are the fluxes of the stationary state \mathbf{U}^* solution of the Riemann problem defined between the cells.

In particular, the approximate-state Riemann solver [44], which is actually exact in this case, is used in this work. The aforementioned solver is constructed upon the introduction of an auxiliary vector \mathbf{Q} , which is taken here as the opposite of $\bar{\mathbf{F}}$, that allows reformulating the Riemann problem (52) by using the chain rule:

$$\mathbf{Q}_t - \frac{\partial \mathbf{Q}}{\partial \mathbf{W}} \mathbf{Q}_x = 0, \quad \text{with} \quad \begin{cases} \mathbf{Q}(x, t = 0) = \mathbf{Q}_L & \text{if } x < 0 \\ \mathbf{Q}(x, t = 0) = \mathbf{Q}_R & \text{if } x > 0 \end{cases} \quad (54)$$

The Jacobian matrix of system (54) admits two right eigenvectors \mathbf{R}^1 and \mathbf{R}^2 , respectively associated with the left and right going wave, that correspond to the columns entries of the matrix \mathbf{R} . The stationary solution of system (54) is computed as:

$$\mathbf{Q}^* = \mathbf{Q}_L + \delta_1 \mathbf{R}^1 = \mathbf{Q}_R - \delta_2 \mathbf{R}^2 \quad (55)$$

where δ_1 and δ_2 are the components of the solution of the following system:

$$\mathbf{R} \cdot \boldsymbol{\delta} = \mathbf{Q}_R - \mathbf{Q}_L \quad (56)$$

Note that the dimension of system (56) makes its analytical solution very easy.

At last, the flux quantities of problem (53) directly follow from equation (55) due to the choice of the auxiliary vector $\mathbf{Q} = -\mathbf{F}$. Once the intercell fluxes have been computed for both Riemann problems, one can advance in time the vector of conserved quantities \mathbf{U}_i according to the discrete equation (53).

5.3. Computation of the source term

The source term of equation (49), which essentially corresponds to the damage evolution problem, leads to the following ODE system:

$$\frac{d\mathbf{U}_i}{dt} = \mathbf{S}(\mathbf{U}_i) \quad \forall i \quad (57)$$

In order to avoid any influence on the CFL condition, this system is solved implicitly by using a backward Euler discretization coupled with a Newton-Raphson method. It is however worth noticing that this system of dimension 3 is *fully local* unlike the so far existing approaches.

The initial conditions used in the solution of (57) depends on the splitting scheme used. Godunov splitting, which is the simplest and the one used in this work, consists in first solving the homogeneous system and in using the computed solution as initial condition of the solution of system (57).

To summarize, the numerical procedure for one time step $\Delta t^n = t^{n+1} - t^n$ and one cell i of length Δx_i is as follows:

- (1) Conservative update: $\mathbf{U}_i^h = \mathbf{U}_i^n - \frac{\Delta t^n}{\Delta x_i} \left(\mathbf{F}_{i+1/2}^* - \mathbf{F}_{i-1/2}^* \right)$
- (2) Solution of the ODE system: $\mathbf{U}_i^{n+1} = \mathbf{U}_i^h + \Delta t \mathbf{S}(\mathbf{U}_i^{n+1})$

6. Numerical results

6.1. Constitutive model

Two different problems will be considered in this section for a one-dimensional domain of length $L = 5$ mm. This solid is assumed to be made of a material for which the free energy density and the yield function are [12, 42]:

$$\begin{aligned} \Psi(\varepsilon, \mathcal{D}, \tilde{\mathcal{D}}, \tilde{\mathcal{D}}_x) &= \frac{A(\mathcal{D})}{2} \varepsilon^2 + w(\mathcal{D}) + \frac{1}{2} \mathbf{w}_l \mathbf{l}_c^2 \tilde{\mathcal{D}}_x^2 + \frac{\kappa}{2} (\tilde{\mathcal{D}} - \mathcal{D})^2, \\ \text{with } A(\mathcal{D}) &= \frac{1}{2} (1 + \text{sgn}(\varepsilon)) E (1 - \mathcal{D})^2 + \frac{1}{2} (1 - \text{sgn}(\varepsilon)) E \\ \text{and } w(\mathcal{D}) &= (1 - \gamma) k_l \mathcal{D} - M_l (\ln(1 - \mathcal{D}) + \mathcal{D}) \\ f_{\mathcal{D}} &= -\frac{\partial \Psi}{\partial \mathcal{D}}(\langle \varepsilon \rangle) - \gamma k_l \end{aligned} \quad (58)$$

E being Young's modulus and sgn the sign function. In this model, $\gamma \in [0, 1]$ is a parameter used to tune the dissipated part of local damage energy, thus providing a general formulation

of the situations discussed in section 4.2. Namely, the damage energy is fully stored for $\gamma = 0$ and fully dissipated for $\gamma = 1$. Note that in any case, one has:

$$f_{\mathcal{D}} = -\frac{A'(\mathcal{D})}{2}\langle\varepsilon\rangle^2 - k_l + M_l\frac{\mathcal{D}}{1-\mathcal{D}} + \kappa(\tilde{\mathcal{D}} - \mathcal{D}) \quad (59)$$

in such a way that for $\kappa \rightarrow \infty$ and $\beta \rightarrow 0$, the criterion commonly used in quasi-static is recovered.

The choices made in terms of free energy density and yield function allows to model unilateral effects with total recovery of the elastic modulus due to microcracks closure, that is, E in compression and $E(1 - \mathcal{D})^2$ in tension. This effect is indeed of major importance in dynamics for the role it plays on the speeds of tension and compression waves.

The microinertia parameter is on the other hand normalized as:

$$\beta = \beta_0 \frac{\rho \mathbf{w}_{l_c} l_c^2}{A(0)} \quad (60)$$

Since there is no reason that any information on damage propagates faster than the acoustic waves in the material, we should have $\beta_0 \geq 1$. The choice is made here to keep this parameter equal to one for every numerical simulations for simplicity. However, the microinertia must be the object of further modeling for it is expected to provide the crack propagation speed when $\mathcal{D} = 1$. This is nonetheless out of the scope of the present paper.

The values of the material parameters used in both numerical simulations are given in table 1. The selected values of the viscosity and the penalty parameters η and κ enable the

E (GPa)	ρ (kg·m ⁻³)	l_c (m)	η (s ⁻¹)	k_l (Pa)	M_l (Pa)	κ (Pa)	\mathbf{w}_{l_c} (Pa)
27	2500	2×10^{-3}	1×10^{-4}	50	250	1×10^6	1

Table 1: Material parameters used for numerical simulations.

computation of qualitative results without encountering any numerical difficulty. A complete analysis of these parameters, which is also out of the scope of the present paper for which the focus is on the model derivation, should nevertheless be done in future works.

6.2. Multi-fragmentation test case

We consider the one-dimensional sample submitted to a uniform in space and time strain rate $\varepsilon_t = \frac{v_d}{L}$. This is done through the combination of Dirichlet boundary conditions and initial conditions on the velocity:

$$v(x = 0, t) = -v_d \quad ; \quad v(x = L, t) = 0 \quad ; \quad v(x, t = 0) = -v_d\left(1 - \frac{x}{L}\right) \quad (61)$$

As depicted in figure 2, this problem can be seen as a one-dimensional modeling of a very thin spherical shell undergoing a constant internal pressure. The setting thus considered is interesting for it allows to get closer from quasi-static conditions.

For the simulations, the nondissipative damage model is selected (*i.e.* $\gamma = 0$) and the CFL number is set to 0.5. The simulations considered in this section ran until the physical time $t = 1.83 \times 10^{-5}$ s is reached, which corresponds to 12 travels across the domain of an elastic wave with speed $c^E(\mathcal{D} = 0)$.

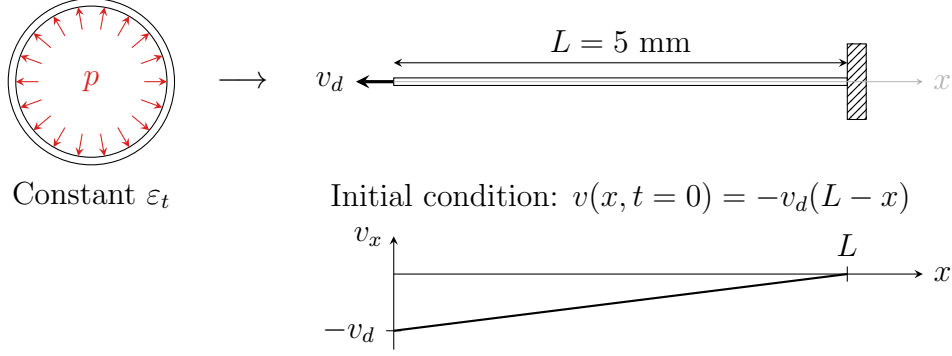


Figure 2: One-dimensional modeling of the dynamic fragmentation of a thin spherical shell.

6.2.1. Dynamical response of the medium

We start the illustration of the proposed model with a coarse mesh made of 50 uniform finite volume cells in order to present the evolution of fields in the medium for an enforced velocity of magnitude $v_d = 0.1$ m/s.

Each row in figure 3 shows the stress or damage variables along the one-dimensional medium at three different times corresponding to the columns. The first phase of the de-

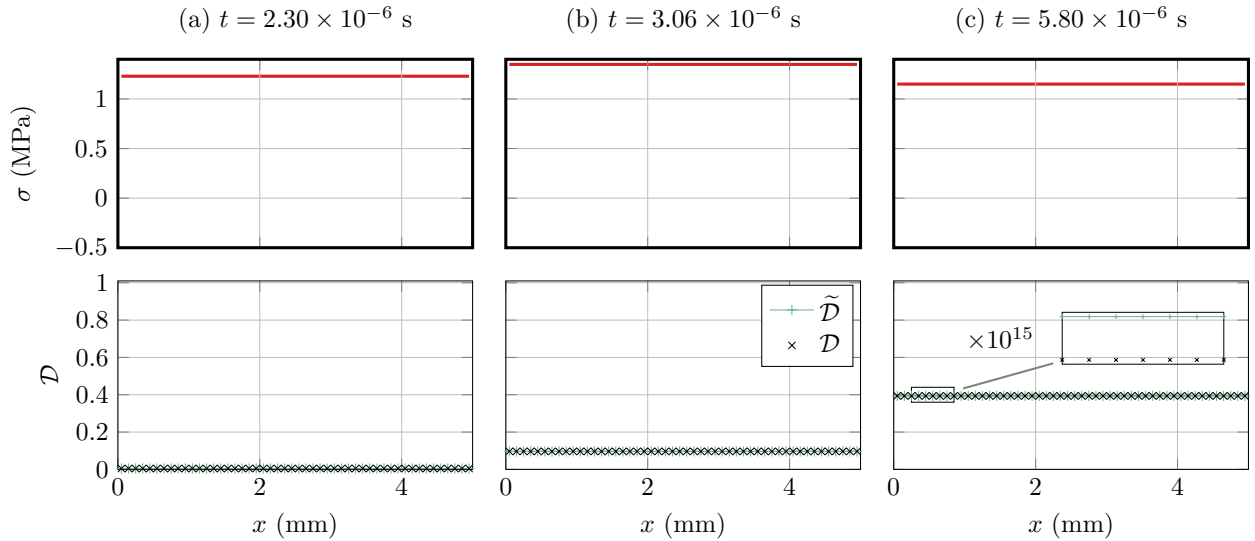


Figure 3: Stress and damage variables along the one-dimensional domain for a computation performed with a 50 cells uniform mesh: $v_d = 0.1$ m/s.

formation is purely elastic in such a way that stress increases homogeneously in the domain until the damage threshold is reached ($f_D \geq 0$), which implies damage flow in every cells. The state depicted in figure 3a corresponds to the very beginning of damage flow though it cannot be distinguished in the plot. In figure 3b, however, one can see that damage flow occurred since the damage variables are approximately equal to 0.1. Notice that the stress continued increasing with respect to the previous time steps. This is consistent with the σ - ε

curve (see that of the left cell provided in figure 4), in which the maximum stress is achieved for $\mathcal{D} > 0$.

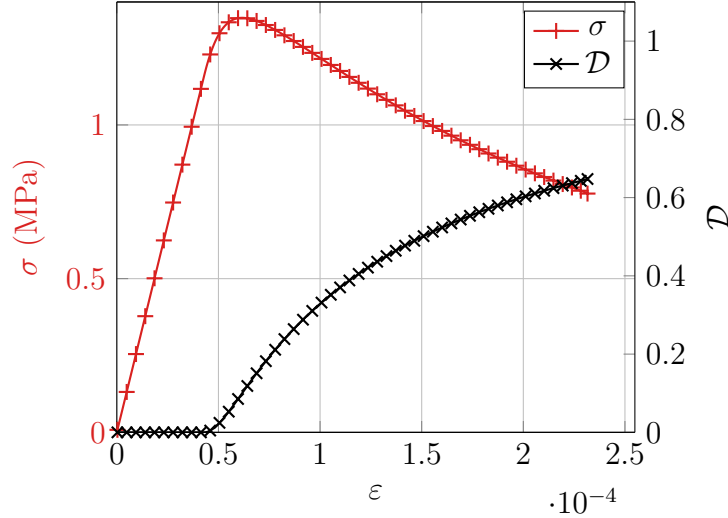


Figure 4: Constitutive model in the first cell of the domain: Left axis for $\sigma(\varepsilon(t))$ curve; Right axis for $\mathcal{D}(\varepsilon(t))$ curve.

The damage variables continue to increase after the stress crossed its maximum value as shown in figure 3c. At that time, damage is still homogeneous. It is also worth noticing that at $t = 5.80 \times 10^{-6}$ s, both damage variables are constant in the domain and the gap between \mathcal{D} and $\tilde{\mathcal{D}}$ is of the order of 10^{-16} as can be seen in figure 3c.

The results of subsequent time steps are presented in figure 5. One can see in figure 5a that heterogeneities that are most likely due to round off errors eventually arise in the damage profiles. As a result, the stress level is no longer constant in the domain. At time $t = 1.31 \times 10^{-5}$ s, several fragments are formed that is, zones where \mathcal{D} is very close to one. However, stress waves continue to propagate in the domain, which is seen in the stress profile in figure 5b. From that time, damage no longer evolves so that no notable changes can be seen between figures 5b and 5c in terms of the damage profile.

6.2.2. Mesh convergence

We now consider finer meshes made of $\{500, 1000, 2000, 4000\}$ cells and four loading conditions depending on the value of the enforced velocity $v_d = \{0.1, 0.2, 0.4, 1.2\}$ m/s to see the effect on the fragmentation of the domain. These loading conditions lead to strain rate values that respectively correspond to $\varepsilon_t = \{20, 40, 80, 240\} s^{-1}$.

Figure 6 shows the damage variable \mathcal{D} profile in the one-dimensional domain at the end of the computation ($t = 1.83 \times 10^{-5}$) for the four considered strain rates. First, the number of fragments at the end of the computation increases with the enforced strain rate as expected. Even though the final damage profile along the one-dimensional domain differs from one mesh size to another, which is not surprising given that the problem is somehow driven by numerical round off error, the results do not differ significantly when the mesh is refined.

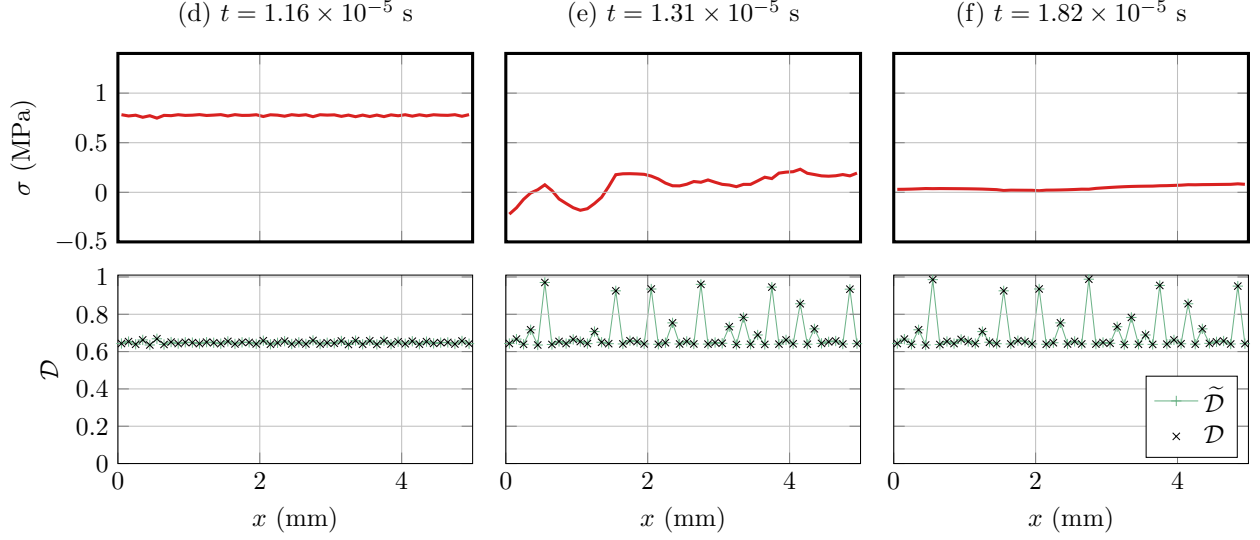


Figure 5: Stress, damage and damage rate along the one-dimensional domain for a computation performed with a 50 cells uniform mesh: $v_d = 0.1$ m/s, $\beta_0 = 1$ (Continuation of figure 3)

Notice however that the damage level globally increases with the number of cells for every imposed strain rate.

The evolution of the average fragment size obtained at the end of the computation when the load is increased and mesh is refined can be seen in figure 7. The fragments length is here defined as the distance between two noncontiguous cells at which $\mathcal{D} > 0.98$. Convergence is here analysed in two different ways. First, the left part of figure 7 plots the evolution of the average fragment size with respect to the imposed strain rate. To plot these curves, additional situations involving higher strain rates have been considered, namely $\varepsilon_t = \{400, 800, 1600, 3200\} s^{-1}$. It is then seen that good convergence is achieved in terms of the mean fragment size with mesh refinement. Note nevertheless that the problem cannot be solved using 500 cells for $\varepsilon_t = 1600$ m/s for in that case the mean fragment length is of the same order as the mesh size $\Delta x = 1 \times 10^{-2}$ mm. Second, the right part of the figure shows that, for a given imposed strain rate, the average fragment size converges with the number of cells for $\dot{\varepsilon} \leq 240 s^{-1}$. For larger values of the imposed strain rate, the numerical model most likely requires more cells to reach convergence.

The mesh refinement performed also enables the analysis of computational times. Figure 8 then plots the simulation wall times with respect to the mesh size. The figure obviously shows that doubling the number of cells leads to a CPU time that is four times bigger. This feature of the scheme, when applied to one-dimensional problems, is due to the full locality of the hyperbolic model proposed in this paper. Indeed, the existing nonlocal formulations, which require the solution of nonlinear systems for the damage evolution, do not enable such a complexity of the order $\mathcal{O}(\Delta x^2)$.

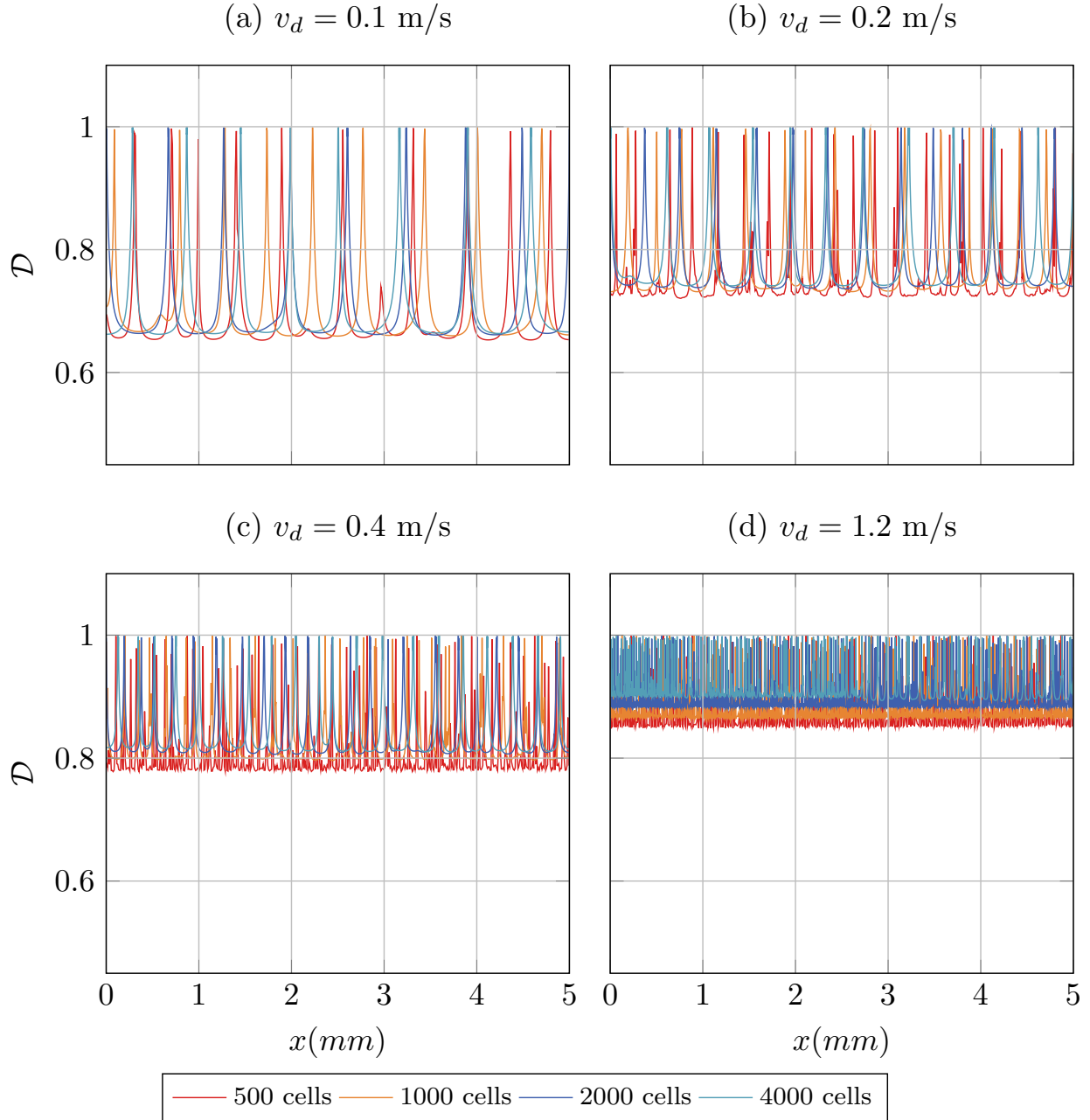


Figure 6: Shell fragmentation test case. Several uniform strain rates ε_t are imposed at $t = 0$ for four different mesh sizes. The damage field \mathcal{D} obtained after $t = 1.83 \times 10^{-5}$ s is plotted along the one-dimensional domain.

6.3. One-dimensional spalling test

We now consider an impact between a projectile and an immobile solid which is modeled in one space dimension by prescribing a positive initial velocity to the left part of the domain and a zero initial velocity to the right part (see figure 9). This setting is well suited to perform

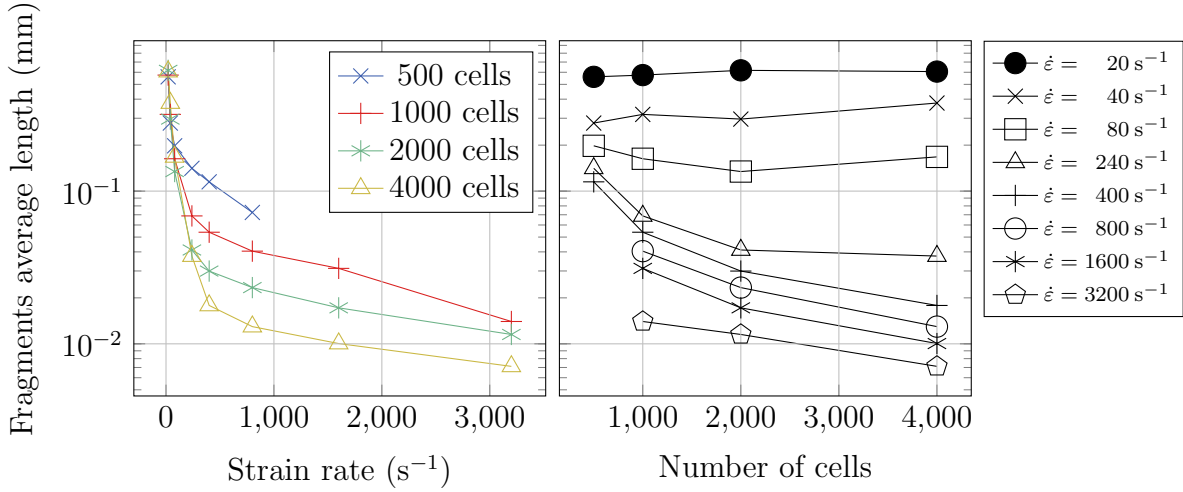


Figure 7: Evolution of the mean fragment size. Left figure: evolution with respect to the imposed strain rate. Right figure: evolution with respect to the number of cells.

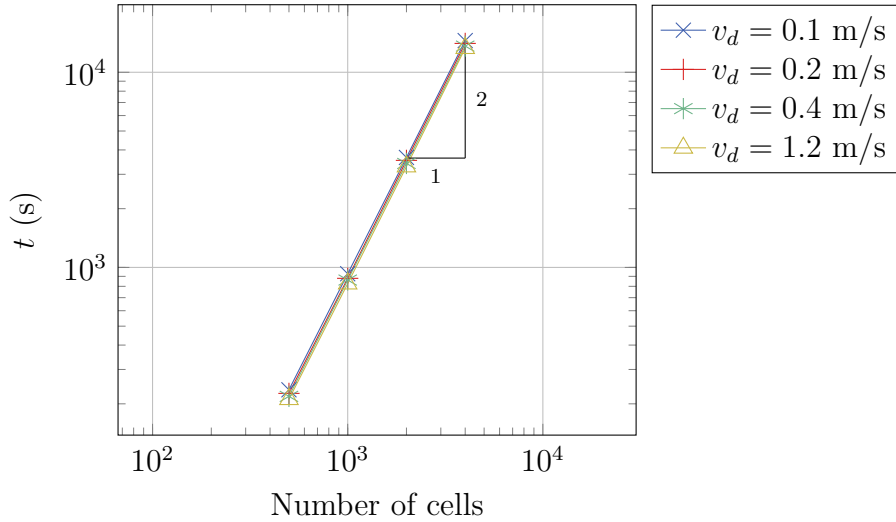


Figure 8: Evolution of the computational time with respect to the number of cells considered for one simulation of the one-dimensional multi-fragmentation test.

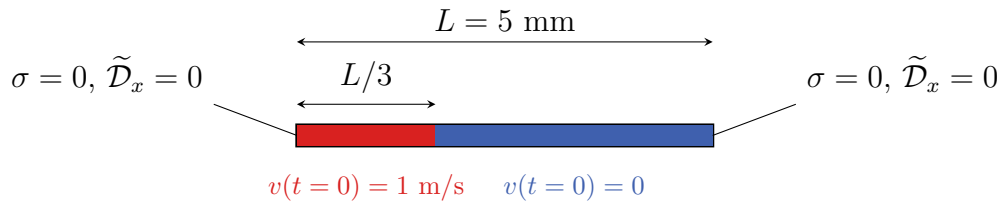


Figure 9: Initial and boundary conditions for the one-dimensional spalling test

one-dimensional simulations of the spalling test or the Laser Shock Adhesion Test.

For the simulations, both the fully dissipative (*i.e.* $\gamma = 1$) and the nondissipative (*i.e.* $\gamma = 0$) have been considered. The physical time of the simulations is $1.5L/c^E(\mathcal{D} = 0)$ and the CFL is set to 1.

6.3.1. Dynamical response of the medium

Figure 10 shows stress and damage profiles along the domain at different times, computed with the dissipative and the nondissipative model. It can thus be seen that the two considered models lead to the same solutions at any times.

The results in terms of stress and damage are presented in two complementary manners. In figure 10, stress and damage profiles along the domain made of 2000 cells are shown at different times while figure 11 displays colormaps of fields in the (x, t) plane. Thus, the plots of figure 10 correspond to slices of figure 11 which are indicated by annotated horizontal lines.

At the beginning of the computation, two compression waves emanate from the velocity discontinuity and propagate toward each end of the domain (see figure 10a). After reflection of the incident waves on the free boundaries, two unloading waves propagate toward the interior of the domain (figure 10b). Those relaxations meet at $x = 2L/3$ and result in two tensile waves moving leftward and rightward. Under that tensile stress state, damage flow is triggered and \mathcal{D} starts increasing, which can be seen in figure 10c. Then, figure 10d shows that the stress level decreases at $x = 2L/3$ as damage increases until the domain completely breaks at that point. Note also that the stress level on the elastic wave front decreased with respect to time $t = 1.58 \times 10^{-6}$ s. This is due to the time required for the stress to go back on the yield surface during the relaxation process. The consequence of that amplitude decay is that the damage flow associated with the tensile waves front yields a damage level that is lower and lower as one looks further from $x = 2L/3$. That point appears as a color gradients along the characteristics in figure 11.

At time $t = 1.83 \times 10^{-6}$ s, the domain broke at $x = 2L/3$ (figure 10e). This leads to the appearance of two white vertical bands in the plots of figure 11 that respectively correspond to $\sigma = 0$ and $\mathcal{D} \approx 1$.

The stress level continues decreasing in the vicinity of the formed crack, thus making the amplitude of the tensile waves lower and lower as indicated by the color gradient in the left plot of figure 11. Eventually, σ becomes negative near the crack, which can be seen as an elastic rebound due to fracture that results in two compression waves propagating left and rightward. This appears as the blue gradient zone near the crack above line (e) in the left plot of figure 11. The algorithm fails in capturing accurately those waves, hence the oscillations that can be seen in figure 10f. Nonetheless, lowering down the CFL number allows avoiding these spurious oscillations.

The presented results then demonstrate the ability to follow waves even once fragments have formed.

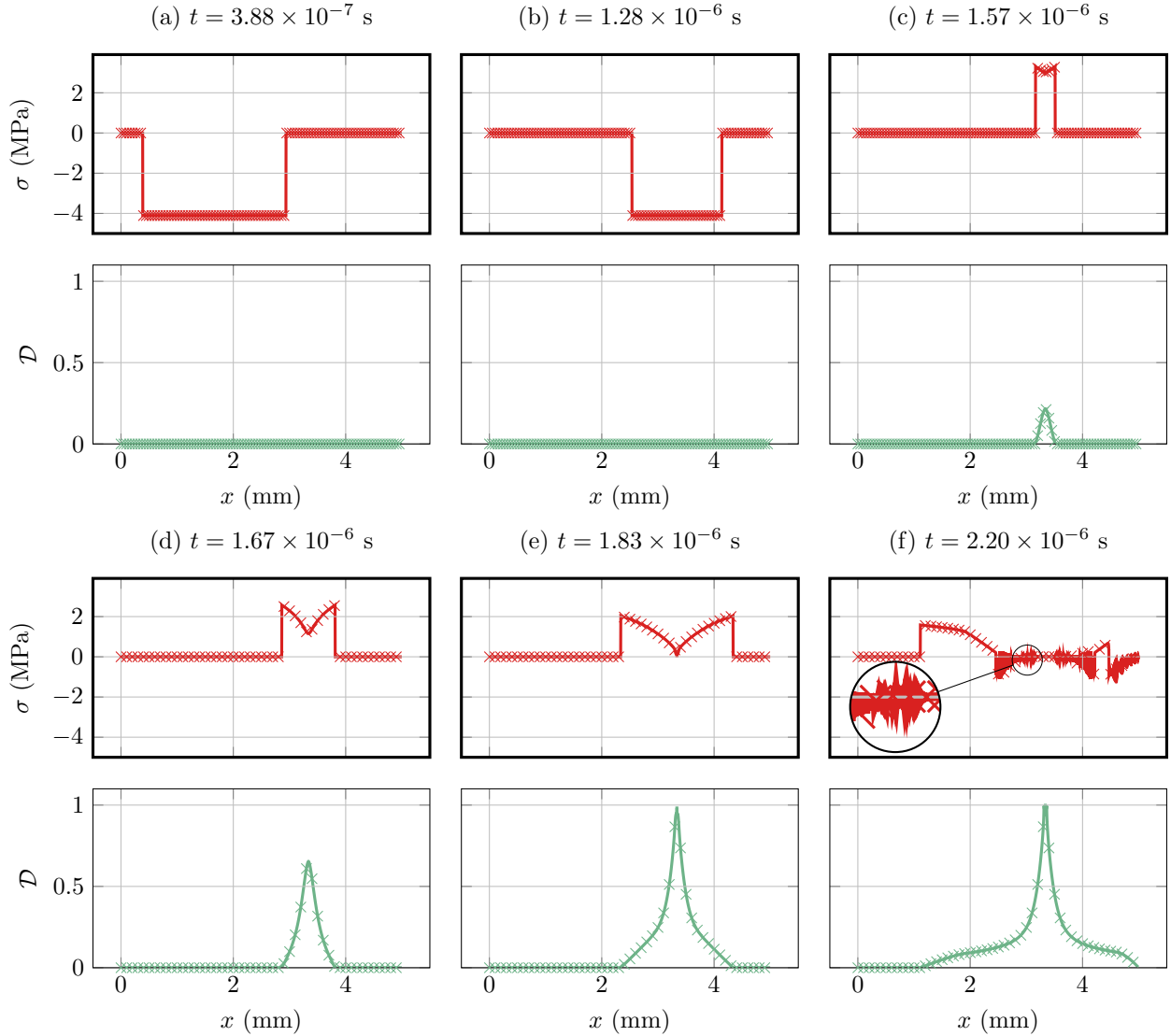


Figure 10: Stress and damage profile along the one-dimensional domain at different times of the spalling test: comparison between the nondissipative model (solid lines) and the dissipative one (markers).

6.3.2. Energy balance

Let us now have a look to the evolution of energy quantities during the simulation shown in figure 12. A comparison between the nondissipative (solid lines) and fully dissipative (markers) cases is proposed in terms of total, kinetic and free energies. As before, the mapping can be made with figure 10 owing to annotated vertical lines.

One sees that no difference between the two settings of the model can be seen before damage flow begins. Indeed, the total energy is conserved in both cases since the CFL is set to 1. After the initiation of damage evolution, however, a gap due to physical dissipation

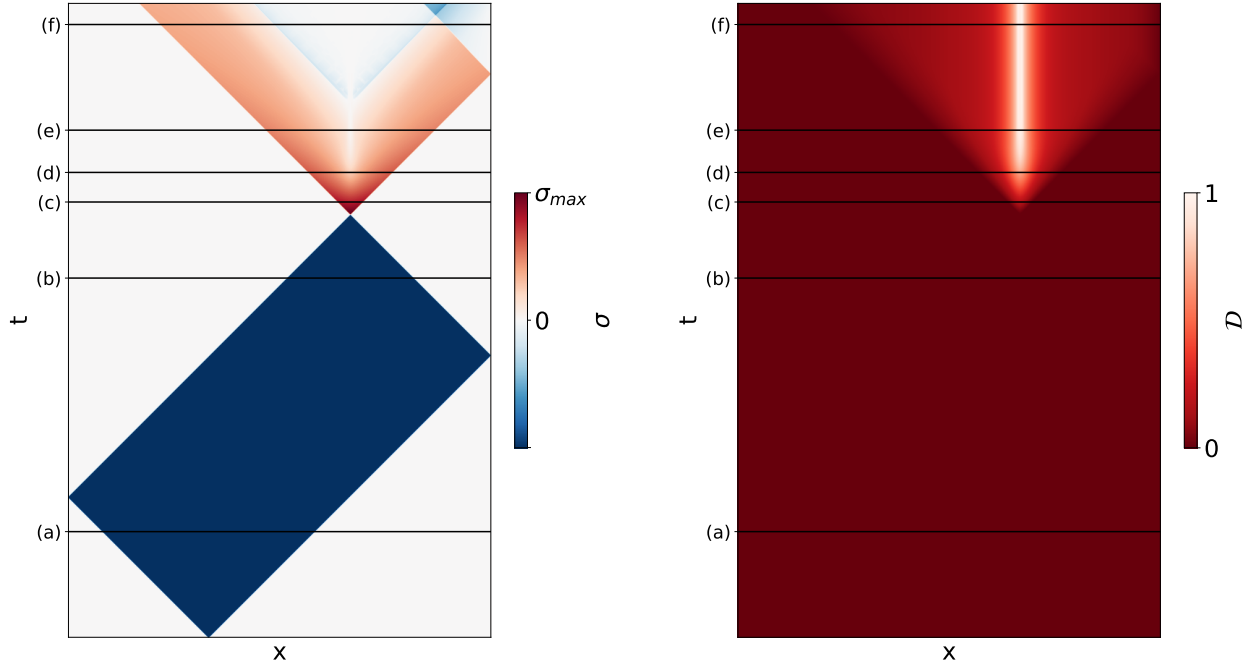


Figure 11: Representation of the solution of the spalling test problem in the (x, t) plane. Left plot: Stress σ ; Right plot: Damage variable D .

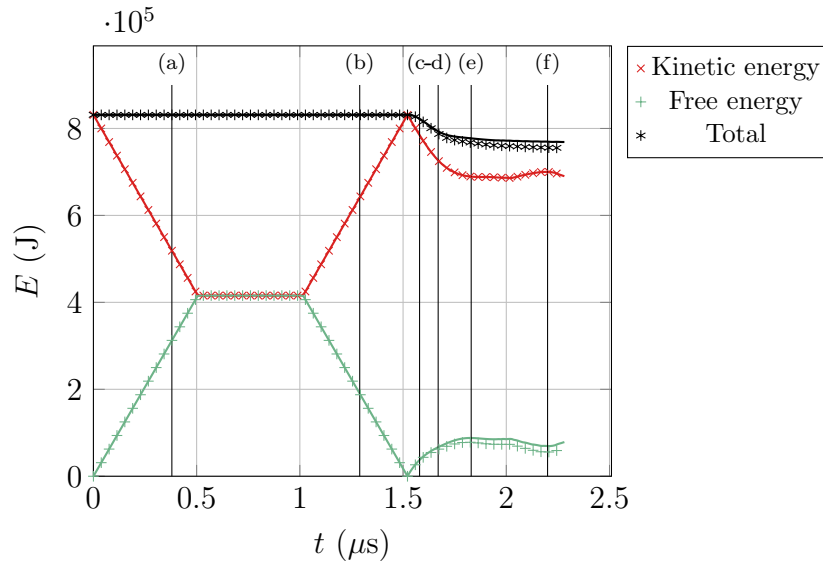


Figure 12: Evolution of total, kinetic and free energies with time: Solid lines stand for the nondissipative model and markers for the fully dissipative one

appears in total and free energy curves. Numerical diffusion also appears as the total energy decay observed in the nondissipative case after damage flow started. This diffusion results from damage that leads to elastic waves travelling with a speed lower than the undamaged

celerity $c^E(\mathcal{D} = 0)$.

Recall that in both cases $\gamma = 0$ and $\gamma = 1$, the same results in terms of stress and damage is obtained. This parameter then enables to tune the dissipation of the model in order to, for instance, fit experimental data without modifying the solution.

7. Conclusion

A new hyperbolic system for modeling dynamic brittle damage and fracture has been introduced for three-dimensional problems. The derivation of the model follows from the application of Hamilton’s variational principle to solids whose internal energy depends on the damage internal variable commonly used and its gradient. According to the extended Lagrangian approach [28–30], a microinertia term as well as an additional damage variable and a penalty term are considered in the action functional. Taking into account microinertia, which is associated with microvoids in [12], leads to the derivation of an hyperbolic system whose numerical solution is cumbersome for explicit dynamics. Hence the introduction of an additional damage variable that leads to a set of (nondissipative) hyperbolic equations that can easily be solved with finite volumes. Those developments have been presented in section 3.

In section 4, a damage evolution law has been added to the model through the introduction of the dual dissipation pseudo-potential. Note that a rate-dependent model is considered in this work for versatility. Depending on the choice of the yield function and the free energy, nondissipative, partially dissipative, or fully dissipative damage evolutions can be considered as emphasized in section 4.2. The contributions of local and nonlocal terms of the free energy to dissipation can also be tuned independently although this point has not been explored here.

The first-order partial differential equations system obtained after a change of variable has been shown to be hyperbolic in section 5. The homogeneous part of the system can therefore be solved numerically by using a finite volume scheme such as Godunov scheme, which has been briefly recalled. On the other hand, the nonhomogeneous part related to the source term of the governing system is dealt with by an ODE solver that is here implicit. In the end, the governing system of equations is solved using a fractional-step method consisting of the conservative update and implicit solutions of the *local* source term at each step of an explicit time discretization.

The presented numerical simulations show that the model allows to follow waves in a brittle medium even after fracture has occurred (*i.e.* $\mathcal{D} \approx 1$). For the multi-fragmentation test case, the numerical results emphasize that no mesh-dependency is seen and mesh convergence is achieved in terms of number of fragments. In addition, the complexity of the numerical scheme used is of the order $\mathcal{O}(\Delta x^2)$, which results from the fully local formulation of the proposed model. At last, the versatility of the model concerning the amount of dissipated energy has been illustrated on the one-dimensional spalling test.

The presented model, which is very promising for dynamic brittle fracture applications, must now be extended to multi-dimensional problems. This will enable comparisons with existing approaches on the Kalthoff-Winkler test [45] for instance. Extension to finite strain

will be considered in a forthcoming paper. In addition to the aforementioned perspectives, the influence of the microinertia parameter should be deeply studied.

8. Acknowledgement:

This research was funded in part by the French National Research Agency (ANR) under the project "ANR-22-CE51-0034-04" BIGBEN. D. K. would like to acknowledge this support. N.F. acknowledge support from the A*MIDEX and the ANR under grants ANR-11-LABX-0092, ANR-11-IDEX-0001-02, and ANR-ASTRID project SNIP ANR-19-ASTR-0016-01. N.F. acknowledge his habilitation thesis jury, J.J. Marigo, C. Farhat, G. De Saxcé, T. Gallouet, R. Abgrall, J.-P. Vila for suggesting to develop the dynamic aspect for damage.

References

- [1] B. Budiansky, J. O'Connell, Elastic moduli of a cracked solid, *International Journal of Solids and Structures* 12 (1976) 81–97.
- [2] J. Lemaître, J. Chaboche, *Mechanics of solid materials*, Cambridge University Press, (1990).
- [3] J.-J. Marigo, Formulation de l'endommagement d'un matériau élastique, *C. R. Acad. Sci. Paris Sér. II* 292 (19) (1981) 1309–1312.
- [4] B. Halphen, Q. Nguyen, On generalized standard materials.[sur les matériaux standards generalises.], *J Mec* 14 (1975) 39–63.
- [5] J. Ju, Isotropic and anisotropic damage variables in continuum damage mechanics, *Journal of Engineering Mechanics* 116 (12) (1990) 2764–2770.
- [6] D. Halm, A. Dragon, A model of anisotropic damage by mesocrack growth; unilateral effect, *International Journal of Damage Mechanics* 5 (4) (1996) 384–402.
- [7] S. Murakami, K. Kamiya, Constitutive and damage evolution equations of elastic-brittle materials based on irreversible thermodynamics, *International Journal of Mechanical Sciences* 4 (1997) 473–486.
- [8] G. Pijaudier-Cabot, Z. P. Bažant, Nonlocal damage theory, *Journal of engineering mechanics* 113 (10) (1987) 1512–1533.
- [9] R. De Borst, A. Benallal, O. Heeres, A gradient-enhanced damage approach to fracture, *Le Journal de Physique IV* 6 (C6) (1996) 491–512.
- [10] R. H. J. Peerlings, R. de Borst, W. A. M. Brekelmans, M. G. D. Geers, Gradient-enhanced damage modelling of concrete fracture, *Mechanics of Cohesive-frictional Materials* 3 (4) (1998) 323–342.

- [11] M. Frémond, B. Nedjar, Damage and gradient of damage: The unilateral phenomenon, Proc. SMiRT12 (12th Structural Mechanics in Reactor Technology) Vol. H (1993) 375–380.
- [12] M. Frémond, B. Nedjar, Damage, gradient of damage and principle of virtual power, International journal of solids and structures 33 (8) (1996) 1083–1103.
- [13] Q.-S. Nguyen, S. Andrieux, The non-local generalized standard approach: a consistent gradient theory, Comptes Rendus Mécanique 333 (2) (2005) 139–145. doi:<https://doi.org/10.1016/j.crme.2004.09.010>.
- [14] E. Lorentz, A. Benallal, Gradient constitutive relations: numerical aspects and application to gradient damage, Computer Methods in Applied Mechanics and Engineering 194 (50) (2005) 5191–5220. doi:<https://doi.org/10.1016/j.cma.2004.12.016>.
- [15] E. Lorentz, S. Andrieux, A variational formulation for nonlocal damage models, International journal of plasticity 15 (2) (1999) 119–138.
- [16] G. Francfort, J.-J. Marigo, Revisiting brittle fracture as an energy minimization problem, Journal of The Mechanics and Physics of Solids - J MECH PHYS SOLIDS 46 (08 1998). doi:[10.1016/S0022-5096\(98\)00034-9](https://doi.org/10.1016/S0022-5096(98)00034-9).
- [17] B. Bourdin, G. Francfort, J. Marigo, Numerical experiments in revisited brittle fracture., Journal of the Mechanics and Physics of Solids (48) (2000) 797–826.
- [18] G. Dal Maso, F. Iurlano, et al., Fracture models as γ -limits of damage models, Commun. Pure Appl. Anal 12 (4) (2013) 1657–1686.
- [19] N. Moës, C. Stolz, P.-E. Bernard, N. Chevaugeon, A level set based model for damage growth: The thick level set approach, International Journal for Numerical Methods in Engineering 86 (3) (2011) 358–380. doi:<https://doi.org/10.1002/nme.3069>.
- [20] N. Chevaugeon, N. Moës, Lipschitz regularization for fracture: The lip-field approach, Computer Methods in Applied Mechanics and Engineering 402 (2022) 115644, a Special Issue in Honor of the Lifetime Achievements of J. Tinsley Oden. doi:<https://doi.org/10.1016/j.cma.2022.115644>.
- [21] B. Bourdin, C. J. Larsen, C. L. Richardson, A time-discrete model for dynamic fracture based on crack regularization, International journal of fracture 168 (2011) 133–143.
- [22] M. J. Borden, C. V. Verhoosel, M. A. Scott, T. J. Hughes, C. M. Landis, A phase-field description of dynamic brittle fracture, Computer Methods in Applied Mechanics and Engineering 217-220 (2012) 77–95. doi:<https://doi.org/10.1016/j.cma.2012.01.008>.
- [23] M. Hofacker, C. Miehe, Continuum phase field modeling of dynamic fracture: variational principles and staggered fe implementation, Int J Fract. (178) (2012) 113–129.

- [24] T. Li, J.-J. Marigo, D. Guilbaud, S. Potapov, Gradient damage modeling of brittle fracture in an explicit dynamics context, *International Journal for Numerical Methods in Engineering* 108 (11) (2016) 1381–1405. doi:<https://doi.org/10.1002/nme.5262>.
- [25] K. Moreau, N. Moes, D. Picart, L. Stainier, Explicit dynamics with a non-local damage model using the thick level set approach, *International Journal for Numerical Methods in Engineering* 102 (12 2014). doi:[10.1002/nme.4824](https://doi.org/10.1002/nme.4824).
- [26] N. Moës, B. Lé, A. Stershic, Fragmentation analysis of a bar with the lip-field approach, *Mechanics of Materials* 172 (2022) 104365. doi:<https://doi.org/10.1016/j.mechmat.2022.104365>.
- [27] T. Heuzé, Lax–wendroff and tvd finite volume methods for unidimensional thermomechanical numerical simulations of impacts on elastic–plastic solids, *Journal of Computational Physics* 346 (2017) 369–388. doi:<https://doi.org/10.1016/j.jcp.2017.06.027>.
- [28] N. Favrie, S. Gavrilyuk, A rapid numerical method for solving Serre–Green–Naghdi equations describing long free surface gravity waves, *Nonlinearity* 30 (7) (2017) 2718.
- [29] F. Dhaouadi, N. Favrie, S. Gavrilyuk, Extended lagrangian approach for the defocusing nonlinear schrödinger equation, *Studies in Applied Mathematics* 142 (3) (2019) 336–358.
- [30] S. Bourgeois, N. Favrie, B. Lombard, Dynamics of a regularized and bistable Ericksen bar using an extended Lagrangian approach, *Int. J. Solids Structures* 207 (2020) 55–69.
- [31] J. Lubliner, On the thermodynamic foundations of non-linear solid mechanics, *International Journal of Non-Linear Mechanics* 7 (3) (1972) 237–254. doi:[https://doi.org/10.1016/0020-7462\(72\)90048-0](https://doi.org/10.1016/0020-7462(72)90048-0).
- [32] G. Maugin, Internal variables and dissipative structures, *J. Non-Equilib. Thermodyn.* 15 (1990) 173–192.
- [33] P. Germain, Q. Nguyen, P. Suquet, Continuum thermodynamics, *Journal of Applied Mechanics* 105 (1983) 1011–1020. doi:[10.1115/1.3167184](https://doi.org/10.1115/1.3167184).
- [34] G. Maugin, *The thermomechanics of nonlinear irreversible behaviors*, World scientific publishing, 1999.
- [35] S. Gavrilyuk, Multiphase flow modeling via Hamilton’s principle. In the book: F. Dell’Isola and S.L. Gavrilyuk, Eds. *Variational models and methods in solid and fluid mechanics*, CISM Courses and Lectures, Vol. 535, Springer, 2012.
- [36] B. J. Plohr, D. H. Sharp, A conservative eulerian formulation of the equations for elastic flow, *Advances in Applied Mathematics* 9 (4) (1988) 481 – 499.

- [37] J. E. Dunn, J. Serrin, On the thermomechanics of interstitial working, in: *The Breadth and Depth of Continuum Mechanics*, Springer, 1986, pp. 705–743.
- [38] A. Molinari, S. Mercier, Micromechanical modelling of porous materials under dynamic loading, *Journal of the Mechanics and Physics of Solids* 49 (7) (2001) 1497–1516.
- [39] A. C. Eringen, E. Suhubi, Nonlinear theory of simple micro-elastic solids—i, *International Journal of Engineering Science* 2 (2) (1964) 189–203.
- [40] S. Forest, Micromorphic approach for gradient elasticity, viscoplasticity, and damage, *Journal of Engineering Mechanics* 135 (3) (2009) 117–131.
- [41] E. Diamantopoulou, W. Liu, C. Labergere, H. Badreddine, K. Saanouni, P. Hu, Micromorphic constitutive equations with damage applied to metal forming, *International Journal of Damage Mechanics* 26 (2) (2017) 314–339.
- [42] Z. Bažant, J. Mazars, *Cracking and Damage: Strain Localization and Size Effect*, Taylor & Francis, 2006.
- [43] R. J. LeVeque, *Finite Volume Methods for Hyperbolic Problems*, Cambridge Texts in Applied Mathematics, Cambridge University Press, 2002. doi:10.1017/CB09780511791253.
- [44] E. F. Toro, *Riemann solvers and numerical methods for fluid dynamics: a practical introduction*, Springer Science & Business Media, 2013.
- [45] J. F. Kalthoff, Modes of dynamic shear failure in solids, *International Journal of fracture* 101 (1-2) (2000) 1–31.